



# Increased conversion and selectivity of 4-nitrostyrene hydrogenation to 4-aminostyrene on Pt nanoparticles supported on titanium-tungsten mixed oxides



Marco Carrus<sup>a,b</sup>, Marzia Fantauzzi<sup>c</sup>, Francesca Riboni<sup>a,d</sup>, Martin Makosch<sup>b</sup>, Antonella Rossi<sup>c,e,\*</sup>, Elena Sell<sup>a,\*\*</sup>, Jeroen A. van Bokhoven<sup>b,f,\*\*</sup>

<sup>a</sup> Dipartimento di Chimica, Università degli Studi di Milano, via Golgi 19, 20133 Milano, Italy

<sup>b</sup> Institute for Chemical and Bioengineering, ETH Zurich, 8093 Zürich, Switzerland

<sup>c</sup> Dipartimento di Scienze Chimiche e Geologiche, Università di Cagliari, 09042 Monserrato (Ca), Italy

<sup>d</sup> Present address: Department of Materials Science WW4-LKO, University of Erlangen-Nuremberg, Martensstrasse 7, 91058 Erlangen, Germany

<sup>e</sup> Laboratory of Surface Science & Technology (LSST), Department of Materials, ETH-Hönggerberg, 8093 Zürich, Switzerland

<sup>f</sup> Swiss Light Source, Paul Scherrer Institute, 5232 Villigen, Switzerland

## ARTICLE INFO

### Article history:

Received 12 January 2016

Received in revised form 13 March 2016

Accepted 29 March 2016

Available online 30 March 2016

### Keywords:

Selective hydrogenation

Reduction of nitro group

Supported Pt

W-Doped TiO<sub>2</sub>

X-ray photoelectron spectroscopy (XPS)

## ABSTRACT

A catalyst series consisting in platinum nanoparticles photodeposited on pure titania and on W/Ti mixed oxides, these latter prepared by the sol-gel method, were tested in the hydrogenation of 4-nitrostyrene. A remarkable increase in the reaction rate occurred when the catalyst support contained tungsten, with a parallel boosting in the selective reduction of the nitro group. With the selective W-containing catalysts, the reaction proceeded at constant rate (zero order rate law), while the tungsten-free catalyst showed a rate-dependence on the 4-nitrostyrene concentration (positive order reaction). The presence of tungsten in the support is beneficial not only because a higher surface area is obtained, thanks to the stabilization of anatase owing to the presence of tungsten, but also because it allows the photodeposition of smaller, better dispersed platinum particles, on which the adsorption of the aromatic part of 4-nitrostyrene is less favored. Tungsten not only substitutes titanium in the titania lattice, as revealed by HAAF-STEM analysis, but it is also present as WO<sub>x</sub> species partly covering the Pt nanoparticles photodeposited on the mixed oxide support, as revealed by an in depth distribution XPS analysis. This accounts for the progressively lower performance observed with increasing tungsten content in the catalysts, the highest conversion and selective hydrogenation of the 4-nitrostyrene nitro group having been achieved on the catalyst with a 1% W/Ti molar ratio.

© 2016 Elsevier B.V. All rights reserved.

## 1. Introduction

The research directed towards the development and improvement of photocatalysts led to the design of new nanomaterials prepared exclusively for photocatalytic applications. In particular, a considerable attention has been paid to titania and its increase in photoactivity as a result of modifying the surface and the bulk by metal and/or nonmetal doping [1,2]. However, titania is a traditional support in thermal catalysis. In particular, platinum [3],

palladium [4], gold [5] and rhenium [3] nanoparticles supported on titania are excellent catalysts in the hydrogenation of aromatic nitro compounds to anilines, with the supported metals acting as catalytic sites. The aminobenzenes obtained by this reaction are important intermediates in the manufacture of many agrochemicals, pharmaceuticals, dyes, and pigments [6–8].

The catalytic hydrogenation of simple aromatic nitro compounds poses only a few problems and is, therefore, implemented on a large scale. However, it is difficult to selectively reduce the nitro group in a catalytic process when other reducible groups are present in the aromatic molecule, especially when hydrogen is employed as reducing agent. Significant effort has, thus, been made to develop more selective catalysts [9], although an increase in selectivity was often accompanied by a decrease in activity. For example, Corma's group [3,10] showed that gold particles, supported on titania or iron oxide, catalyze the reduction of various

\* Corresponding author at: Dipartimento di Scienze Chimiche e Geologiche, Università di Cagliari, 09042 Monserrato (Ca), Italy.

\*\* Corresponding authors.

E-mail addresses:

[rossi@unica.it](mailto:rossi@unica.it), [antonella.rossi@mat.ethz.ch](mailto:antonella.rossi@mat.ethz.ch) (A. Rossi), [elena.sell@unimi.it](mailto:elena.sell@unimi.it) (E. Sell), [jeroen.vanbokhoven@chem.ethz.ch](mailto:jeroen.vanbokhoven@chem.ethz.ch) (J.A. van Bokhoven).

functionalized aromatic nitro compounds with high chemoselectivity and without the unwanted accumulation of explosive phenyl hydroxylamine byproducts. Selectivity was successfully addressed in another way, i.e. by modifying the platinum deposited on titania with organic thiols to affect the adsorption mode and control selectivity [11], or by the use of soluble nanoparticles poisoned with phosphine ligands or self-assembled monolayers [12]. A recent review paper addressed how chemoselectivity to nitro group reduction can be induced in traditionally unselective metals by controlling the architecture of the metal catalysts, avoiding the addition of toxic substances [13].

We have taken a different approach in the present work, the goal of which is to ascertain whether the composition of the support affects the conversion and selectivity of the reaction. The selective catalytic reduction of the nitro group of 4-nitrostyrene was, thus, investigated over platinum nanoparticles, photodeposited on titanium-tungsten mixed oxides with W/Ti molar ratios in the 0–0.05 range, prepared by the sol-gel method. There was an increase in the reaction rate and in selectivity to 4-aminostyrene when doping with tungsten was optimal. A detailed investigation of the materials by different techniques made it possible to correlate the activity and selectivity to the composition of the active platinum nanoparticles, the structure of which is affected by the presence of tungsten.

## 2. Experimental

### 2.1. Synthesis of the supporting materials

A pure  $\text{TiO}_2$  sample, labeled as TW0, was synthesized by a sol-gel method, starting from titanium(IV) isopropoxide (TTIP Aldrich, purity 97%) as the titanium precursor, according to a procedure similar to that described elsewhere [14]. An anhydrous ethanol solution ( $100 \text{ cm}^3$ , purity > 99.8%) containing  $10 \text{ cm}^3$  of dissolved TTIP was heated at  $30^\circ\text{C}$  under vigorous stirring. Then  $34 \text{ cm}^3$  of water were added dropwise in order to obtain a molar ratio of  $\text{Ti}/\text{H}_2\text{O} = 1/58$ .

Tungsten-doped  $\text{TiO}_2$  samples were obtained by adding the required amount of tungsten(VI) hexa-ethoxide ( $\text{W}(\text{OC}_2\text{H}_5)_6$ , Alfa-Aesar 99.8%, 5 wt.% in ethanol) to the TTIP ethanol solution to obtain nominal W/Ti molar ratios of 1.0, 3.0 and 5.0%. These catalysts were labeled TW $x$ , with  $x$  referring to the W/Ti percent molar ratio.

After stirring and refluxing for 1 h, the suspensions were concentrated under reduced pressure at  $35^\circ\text{C}$ . The resulting white slurries were kept in an oven at  $70^\circ\text{C}$  overnight to eliminate organic compounds and then calcined at  $500^\circ\text{C}$  in a  $100\text{-cm}^3 \text{ min}^{-1}$  airflow for 4 h. All solutions were prepared with ultra-pure water ( $18.2 \text{ M}\Omega \text{ cm}$ ), supplied by a Millipore Direct-Q3 water purification system.

### 2.2. Platinum deposition

Platinum nanoparticles were photo-deposited on the oxide powders according to the procedure described elsewhere [15], starting from 6 vol.% of methanol/water suspensions containing  $3 \text{ g dm}^{-3}$  of oxide powder and the amount of  $\text{H}_2\text{PtCl}_6$  (Aldrich) to obtain a 0.5 wt.% nominal metal loading.  $\text{Pt}^{IV}$  photo-reduction was achieved by irradiating the suspensions for 2 h in a  $15 \text{ cm}^3 \text{ min}^{-1}$  nitrogen flow by means of an immersion fluorescent, low-pressure mercury arc lamp. Platinum-modified powders (PtTW $x$ ) were recovered after at least three cycles of centrifugation, each followed by washing with water, up to the complete removal of residual ions and organic precursors. The samples were dried at  $70^\circ\text{C}$  for one day and stored in the absence of light and humidity.

### 2.3. Catalysts characterization

X-ray powder diffraction (XRPD) measurements were performed with a Philips PW3020 powder diffractometer, operating at 40 kV and 40 mA, and  $\text{Cu K}\alpha$  radiation ( $\lambda = 1.54056 \text{ \AA}$ ) as the X-ray source. The diffractograms were recorded by continuous scanning between  $20^\circ$  and  $80^\circ$   $2\theta$  angles with a  $0.05^\circ$  step. Quantitative phase analysis was carried out according to the Rietveld refinement method with the GSAS software, as described elsewhere [16]. The average crystallite size was obtained by applying the Scherrer equation. The detection limit of the technique is estimated to be equal to 1%.

X-ray photoelectron spectroscopy (XPS) experiments were performed by means of a PHI Quantera SXM spectrometer (ULVAC PHI, Chanhassen, MN, USA) and an  $\text{Al K}\alpha$  radiation ( $\lambda = 1486.6 \text{ eV}$ ) monochromatic source with a beam diameter ranging from 9 to  $200 \mu\text{m}$ . Photoelectron spectra were recorded in fixed analyzer transmission mode. The binding energies were referred to the C 1s peak at 285.0 eV. XPS analysis was performed on pure  $\text{PtO}_2$ ,  $\text{WO}_3$  (both purchased from Aldrich) and  $\text{TiO}_2$  (the TW0 sample), and on PtTW0, PtTW1, PtTW3 and PtTW5. A detailed description of the instrument and of the calibration procedure can be found elsewhere [17].

Energy dispersive X-ray (EDX) spectroscopy experiments, carried out using a Zeiss Sigma Scanning Electron Microscope, equipped with a Bruker Quantax 400 EDS detector ( $30 \text{ mm}^2$  X Flash silicon drift detector), provided information about the surface composition of the catalysts.

Scanning transmission electron microscopy (STEM) measurements were performed on an aberration-corrected HD-2700CS Hitachi STEM microscope operated at an acceleration potential of 200 kV (electron gun: cold-field emitter) with an annular dark field detector (HAADF). Analytical investigations of selected spots and areas were performed in the normal mode with an energy dispersive X-ray spectrometer (EDX, Genesis Spectrum version 6.2 (EDAX)) attached to the microscope. A few drops of the material, suspended in ethanol, were deposited onto a perforated carbon foil supported on a copper grid. After drying, the grid was mounted on the single tilt holder of the microscope.

The specific surface area of the materials was determined by  $\text{N}_2$  adsorption in a Micromeritics Tristar II 3020 V1.03 apparatus according to the Brunauer, Emmett and Teller (BET) method. The samples were pre-treated at  $300^\circ\text{C}$  for 4 h in vacuo.

### 2.4. 4-Nitrostyrene hydrogenation

All hydrogenation runs were performed in  $50\text{-cm}^3$  Premex stainless steel autoclaves [12] with polyetheretherketone inlets. The typical reaction mixture consisted of solvent (20 g, toluene, puriss > 99%, Fluka Analytical), an internal standard (1 mmol mesitylene > 99%, Sigma Aldrich), PtTW $x$  ( $x = 0, 1, 3, 5$ ) catalyst (50 mg) and substrate (0.67 mmol 4-nitrostyrene > 95%, TCI). An autoclave was filled with this mixture, sealed and purged three times with  $\text{H}_2$  under stirring. The autoclave was then pressurized to 10 bar by using  $\text{H}_2$  and heated to  $80^\circ\text{C}$  under constant stirring to start the reaction. Samples were taken at fixed time intervals by means of a sample tube. The samples were filtered and analyzed in an Agilent 7820 gas chromatograph equipped with an apolar 30 m HP 5 MS column. The temperature program consisted of  $20^\circ\text{C min}^{-1}$  heating steps from 80 to  $300^\circ\text{C}$  at a 60/l split ratio. Activity results are expressed in terms of 4-nitrostyrene conversion (moles reacted over the initial number of moles) and selectivity to 4-aminostyrene (moles of 4-aminostyrene produced over the moles of reacted 4-nitrostyrene).

**Table 1**

BET specific surface area (SSA), anatase crystallite dimensions ( $d_A$ ), percent amount of platinum atoms ( $at_{Pt}$ ) and W/Ti percent molar ratio in the investigated catalysts.

Sample	SSA (m <sup>2</sup> /g)	$d_A$ (nm) <sup>a</sup>	$at_{Pt}$ (%) <sup>b,c</sup>	(W/Ti) × 100 <sup>b,c</sup>
PtTW0	40	13	0.39 (0.04)	0
PtTW1	206	6	0.20 (0.04)	1.0 (0.1)
PtTW3	202	5	0.3 (0.1)	3.3 (0.2)
PtTW5	198	6	0.20 (0.04)	5.3 (0.3)

<sup>a</sup> obtained from XRD analysis.

<sup>b</sup> obtained from XPS analysis.

<sup>c</sup> standard deviation (in parentheses) calculated over three independent XPS measurements.

### 3. Results and discussion

#### 3.1. Catalysts characterization

**Table 1** gives the results of BET, XRD and XPS analyses of the investigated catalysts. XRD patterns (Fig. S1 in the Supplementary material) demonstrate that the photo-deposition of platinum nanoparticles did not modify the phase composition of the support, which consisted of pure anatase in both pure titania and tungsten-containing titania samples. The crystallite dimensions, calculated from XRD data by means of the Scherrer equation, indicate a remarkable decrease in the particle size of anatase in samples containing tungsten, with respect to pure titania (**Table 1**). At the same time, the tungsten-containing titania samples had a much larger BET surface area. The W/Ti percentage molar ratios, obtained by XPS analysis, were in excellent agreement with the expected values within the range of experimental uncertainty.

There was no evidence of a crystalline phase corresponding to the formation of pure tungsten trioxide in the XRD spectra of tungsten-containing samples, indicating that tungsten trioxide may be amorphous or may be present in a concentration below the detection limit of XRD (LOD = 1%). Moreover, tungsten ions may be easily incorporated into the titania lattice, either by substituting titanium ions to form W-O-Ti bonds or by being located at interstitial sites. W<sup>6+</sup> can substitute Ti<sup>4+</sup> in the titania lattice, the ionic radius of W<sup>6+</sup> being 0.060 nm and that of Ti<sup>4+</sup> 0.0605 nm [18].

The TEM micrographs of the TW0 and PtTW0 samples (**Fig. 1**) confirm that pure titania crystallites are larger than 10 nm, in agreement with the XRD results (**Table 1**). Nano-sized platinum particles (2–5 nm) are visible after platinum photo-deposition (**Fig. 1b**).

EDX maps were acquired for the PtTW0 sample (Fig. S2 in the Supplementary material) and confirm the presence of platinum nanoparticles (**Fig. S2c**).

The HAAF-STEM images of the investigated titanium-tungsten mixed oxide materials (**Fig. 2**) show the nanoparticles before and after the photo-deposition of platinum nanoparticles. On average, the oxide particles size appears to be less than half that of pure TW0 and PtTW0 (see for example Figs. 2 b vs 1), confirming the  $d_A$  values reported in **Table 1**. Furthermore, all images, in particular those obtained from platinum-free samples, prove the presence of atomically dispersed tungsten, revealed as bright spots in the titania bulk. With increasing tungsten amount, the number of bright spots increases (**Fig. 2a** to c). The bright spots (W) are on the bright lines, thus showing that W is substituting Ti (**Fig. 2c**). The homogeneity of the observed W dispersion leads to the conclusion that W probably resides both in the TiO<sub>2</sub> lattice and on the oxide surface, where it can interact with platinum and/or influence the 4-nitrostyrene hydrogenation reaction. Larger (1.5–2 nm) bright spots appear in the images obtained for the same samples after platinum photo-deposition (**Fig. 2d–f**), confirming the presence of nanometer-sized platinum particles on the surface of the PtTWx catalysts. Notably, the platinum nanoparticles deposited on the mixed oxides are smaller in size (1–2 nm, with the exception of PtW5, the nanoparticles of which are 1–3 nm) than those which were photo-deposited on PtTW0 (2–5 nm) (**Figs. 1 and 2**).

A detailed EDX analysis, performed on a slightly larger (about 3 nm in diameter) metal nanoparticle on the surface of the PtW5 sample (**Fig. 3**, upper panel) demonstrates the presence of both platinum and tungsten in this nanoparticle and support the existence of direct interactions between platinum and tungsten. However, this was not proven in the case of the PtTW1 and PtTW3 samples, probably because of their rather low tungsten content, below the sensitivity of the EDX instrument. The very high dispersion of tungsten visible in the STEM monographs of **Fig. 2** also points to platinum and tungsten to be in close proximity.

XPS characterization was then carried out to determine the composition of all PtTW samples, and, in particular, to check the presence of tungsten in PtTW1 and PtTW3 as well. This technique detects low concentrations of tungsten and gives insight into the chemical composition and oxidation state of surface elements.

**Fig. 4** presents the X-ray photoelectron survey spectra. Signals from all the elements in the catalysts (titanium, oxygen, platinum and tungsten) were detected, together with small amounts of carbon due to organic contamination. Table S1 (Supplementary material) gives the surface composition of the materials. The W/Ti ratios (**Table 1**) are in good agreement with the expected values ( $\pm 10\%$  accuracy). Reproducible XPS analyses of the samples were repeated 18 months after the first acquisition.

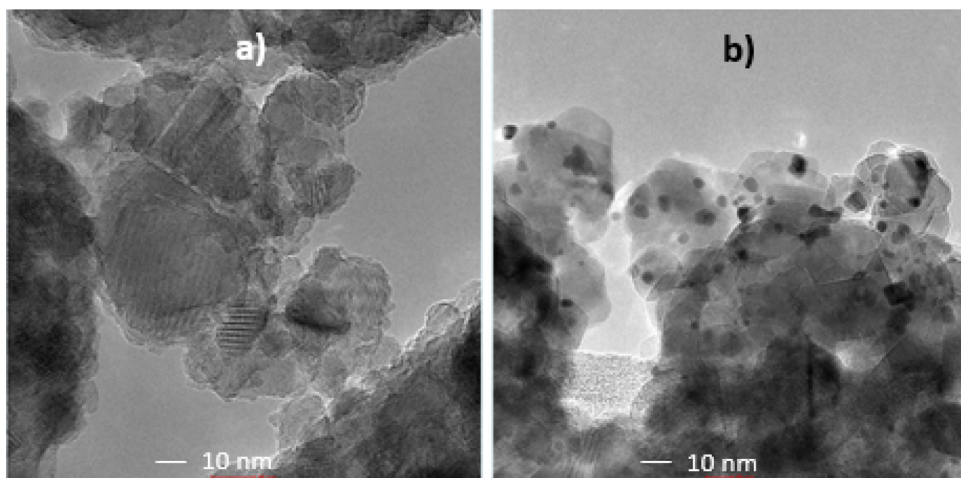


**Fig. 1.** TEM images of (a) TW0 and (b) PtTW0.

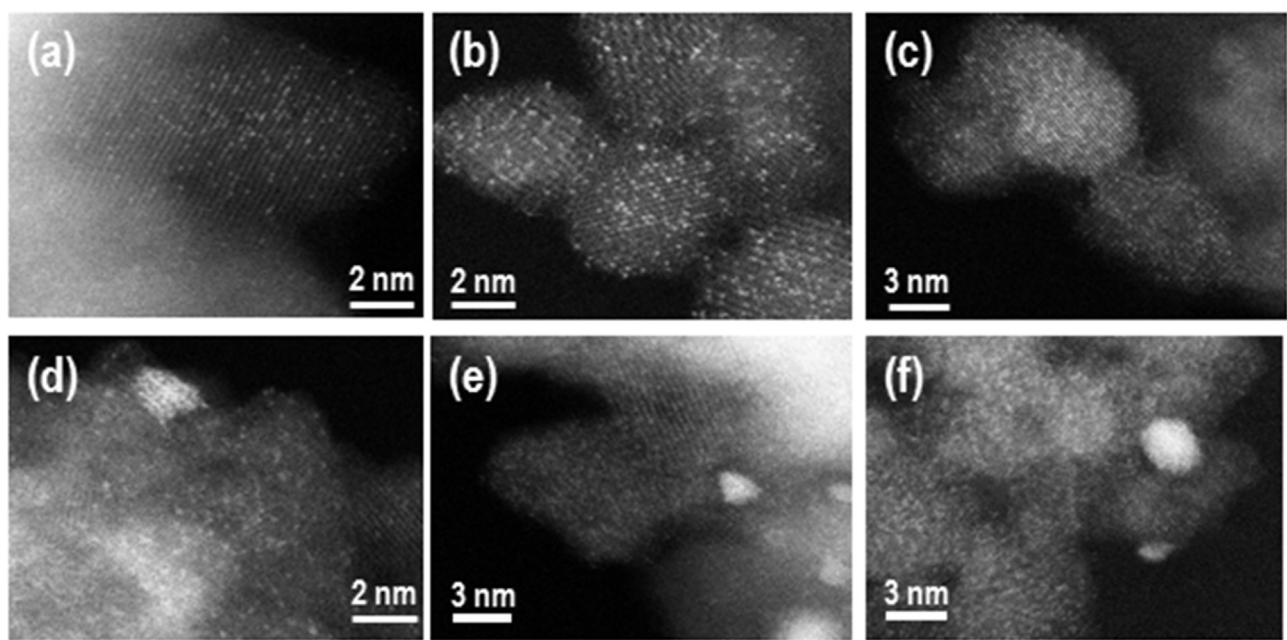


**Fig. 2.** HAAF-STEM images of (a) TW1, (b) TW3, (c) TW5, (d) PtTW1, (e) PtTW3, (f) PtTW5.

**Table 2**

Binding energy (eV) of the main photoelectron peak determined by curve fitting after iterative Shirley-Sherwood background subtraction.<sup>a</sup>

	Ti 2p <sub>3/2</sub>	Ti 3p	W 4f <sub>7/2</sub>	Pt 4f <sub>7/2</sub>	O 1s <sup>b</sup>
TW0	459.0 (0.1)	37.5 (0.1)	–	–	O <sup>2-</sup> = 530.3 (0.1) – 79% OH <sup>-</sup> = 531.5 (0.1) – 13% H <sub>2</sub> O <sub>ads</sub> = 532.7 (0.1) – 8%
PtTW0	459.0 (0.1)	37.5 (0.1)	–	Pt <sup>0</sup> = 70.7 (0.1) Pt <sup>IV</sup> = 73.9 (0.1)	O <sup>2-</sup> = 529.7 (0.1) – 88% OH <sup>-</sup> = 530.7 (0.1) – 7% H <sub>2</sub> O <sub>ads</sub> = 531.7 (0.1) – 5%
PtTW1	459.2 (0.2)	37.6 (0.2)	36.2 (0.2)	Pt <sup>0</sup> = 71.0 (0.2) Pt <sup>IV</sup> = 74.2 (0.1)	O (1) = 530.3 (0.1) – 81% O (2) = 531.0 (0.1) – 12% O (3) = 532.2 (0.1) – 7%
PtTW3	459.2 (0.2)	37.7 (0.2)	36.1 (0.2)	Pt <sup>0</sup> = 71.0 (0.2) Pt <sup>IV</sup> = 74.4 (0.2)	O (1) = 530.3 (0.1) – 79% O (2) = 531.0 (0.1) – 14% O (3) = 532.3 (0.1) – 7%
PtTW5	459.1 (0.1)	37.6 (0.1)	36.1 (0.1)	Pt <sup>0</sup> = 71.0 (0.1) Pt <sup>IV</sup> = 74.3 (0.2)	O (1) = 530.3 (0.1) – 78% O (2) = 531.0 (0.1) – 14% O (3) = 532.2 (0.1) – 8%

<sup>a</sup> Binding energies are given as the mean of three or more independent measurements with the corresponding standard deviations (in parentheses).

<sup>b</sup> The percentage O 1s photoelectron peaks is also reported.

Furthermore, high-resolution XPS spectra were acquired to exploit the unique capability of XPS to provide information about the chemical state of the elements. The spectra of Ti 2p, W 4d and of W 4f, Pt 4f and O 1s were curve-fitted by means of model functions with the same parameters as the pure oxides. Curve fitting parameters, such as the Gaussian-Lorentzian ratio of the product function and the full width at half maximum of the peak height, were kept constant during data processing, while the binding energy and the area of the peaks were not. Table 2 gives the binding energy (BE) of the main photoelectron signals together with the assignment to the respective chemical states.

Ti 2p<sub>3/2</sub> peaks (Fig. 4) of samples without W consist of a single component at 459.0 eV. The single component is assigned to TiO<sub>2</sub>, in agreement with literature data [19,20]. The BE shift in tungsten-containing samples is within the experimental error.

Fig. 5 reports the O 1s and Pt 4f high-resolution XPS spectra. O 1s signals in pure TiO<sub>2</sub> have three components. The most intense one, at 530.3 eV, is ascribed to O in TiO<sub>2</sub>, which also has a component

due to hydroxyl species [21] at 531.5 eV and a third peak at 532.7 eV due to absorbed water (see TW0 in Table 2).

Upon photo-deposition of platinum nanoparticles, all O 1s components undergo a shift to lower binding energy (sample PtTW0 vs sample TW0), with the component at 531.5 eV shifting to 530.7 eV ( $\Delta = -0.8$  eV) in PtTW0.

In tungsten-containing samples, the most intense O 1s component is at 530.3 eV and is due to TiO<sub>2</sub> together with a component at 531.0 eV, which is ascribed to WO<sub>3</sub>, and a small shoulder at 532.2 eV. The intensity of the component at 531.0 eV increases, as expected, with increasing tungsten content in the oxide support.

Pt 4f peaks (Fig. 5, right panels) consist of two doublets (Pt 4f<sub>7/2</sub> and Pt 4f<sub>5/2</sub>), separated by 3.35 eV, with an intensity ratio of 4:3. The most intense doublet at  $71.0 \pm 0.2$  eV, in agreement with values reported in the literature, is assigned to nano-sized platinum supported on oxides such as SiO<sub>2</sub> [22], TiO<sub>2</sub> and WO<sub>3</sub>. Strong metal support interactions occurred in such systems [23]. When platinum nanoparticles smaller than 5 nm are not supported on oxides, there is a positive shift [24] compared to platinum powders [25,26]. The

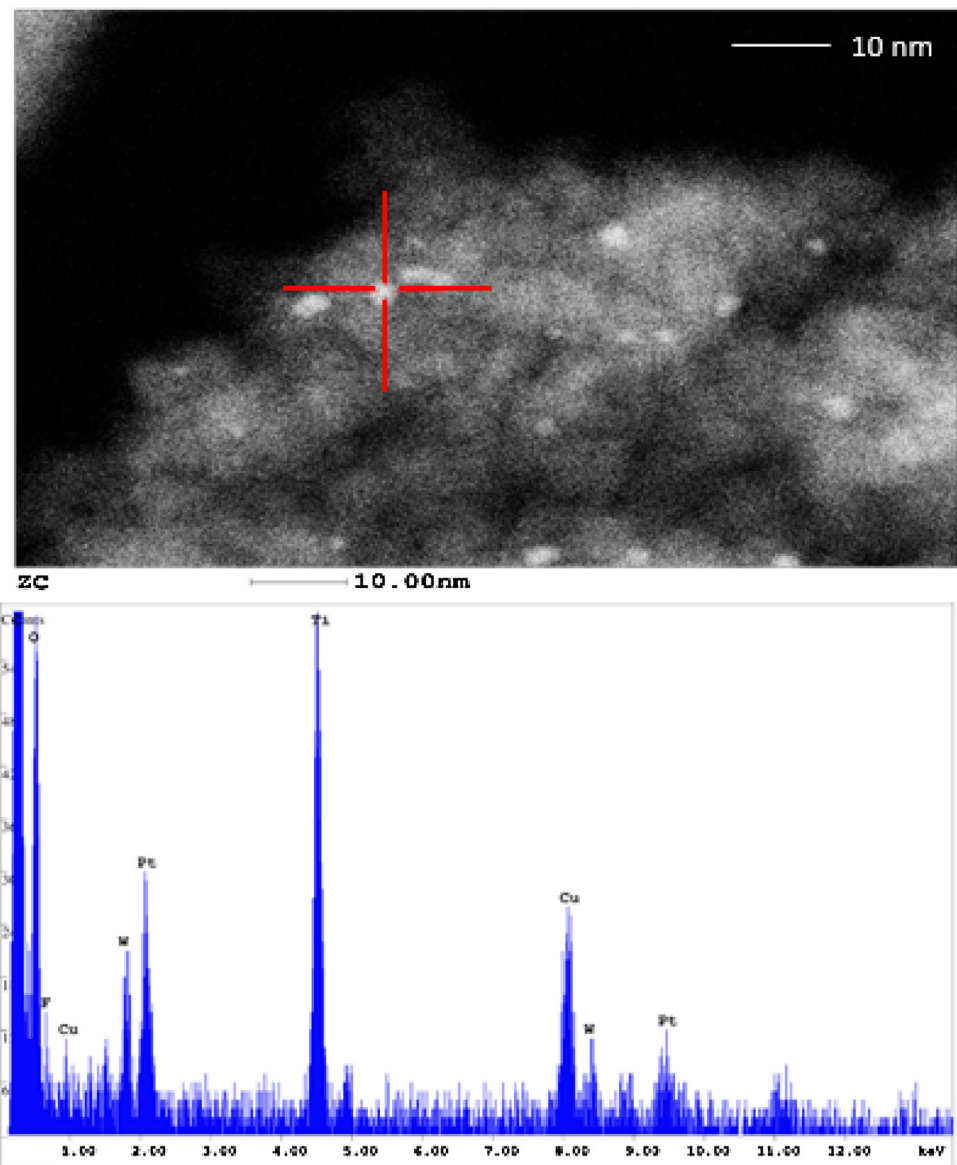


**Fig. 3.** EDX spectrum (lower panel), recorded by focusing on the red cross in the upper panel of the HAAF-STEM image of PtTW5. The copper signal originates from the copper grid. (For interpretation of the references to colour in this figure legend, the reader is referred to the web version of this article.)

doublet at about 74.4 eV is assigned to small amounts of  $\text{PtO}_2$  ( $\text{Pt}^{\text{IV}}$ ) on the surface of the samples [24,27]. The  $\text{Pt}^{\text{IV}}/\text{Pt}^0$  ratio in PtTW0 is 0.14 and is affected by the presence of tungsten in the oxide support; the ratios in PtTW1, PtTW3 and PtTW5 are 0.22, 0.07 and 0.06, respectively. A third component is visible in the Pt 4f region, labeled Ti 3s SAT in Fig. 5. It falls at 76 eV and is a charge transfer shake-up satellite accompanying the photoionization from the Ti 3s orbital [28].

The most intense W peak, W 4f, is found at 36.1 eV; overlap with the Ti 3p peak (BE = 37.6 eV) is shown in Fig. 4. The binding energy of W 4f is in agreement with that for  $\text{WO}_3$  [29]. No shifts dependent on the Ti/W ratio were observed.

### 3.2. Catalytic activity in 4-nitrostyrene hydrogenation

With the  $\text{Pt}/\text{TiO}_2$  (PtTW0) catalyst, the concentration of 4-nitrostyrene decreased exponentially over time, with no 4-nitrostyrene left after about 60 min (Fig. 6a). The main product was 4-ethylnitrobenzene and smaller amounts of 4-ethylaniline were detected in the reaction system about 10 min after the start

of the run. The production rate of 4-ethylnitrobenzene was always higher than that of 4-ethylaniline. After a longer reaction time (not shown), all 4-ethylnitrobenzene was converted into fully hydrogenated 4-ethylaniline, the final reduction product. The carbon balance was always close to 100%, indicating that almost no side reactions occurred. Finally, only more or less negligible amounts of 4-aminostyrene were detected during the runs. The exponential decay and the initial high selectivity to 4-ethylnitrobenzene agree with previous studies with a  $\text{Pt}/\text{TiO}_2$  catalyst [11], even though that catalyst had smaller platinum particles (1–1.5 nm).

In contrast, there was high selectivity to 4-aminostyrene with all W-containing PtTW $x$  ( $x > 0$ ) catalysts, together with a four-fold higher conversion rate of 4-nitrostyrene (Table 3); significant production of 4-ethylstyrene was observed in parallel (Fig. 6b). The concentration of 4-nitrostyrene decreased linearly, not exponentially, which suggests that, with this catalyst, the surface concentration of the reactant is much higher, resulting in zero-order behavior. The best performance was achieved with PtTW1, with 66% selectivity to 4-aminostyrene at 80% conversion, more than six times higher than that obtained with PtTW0. When the

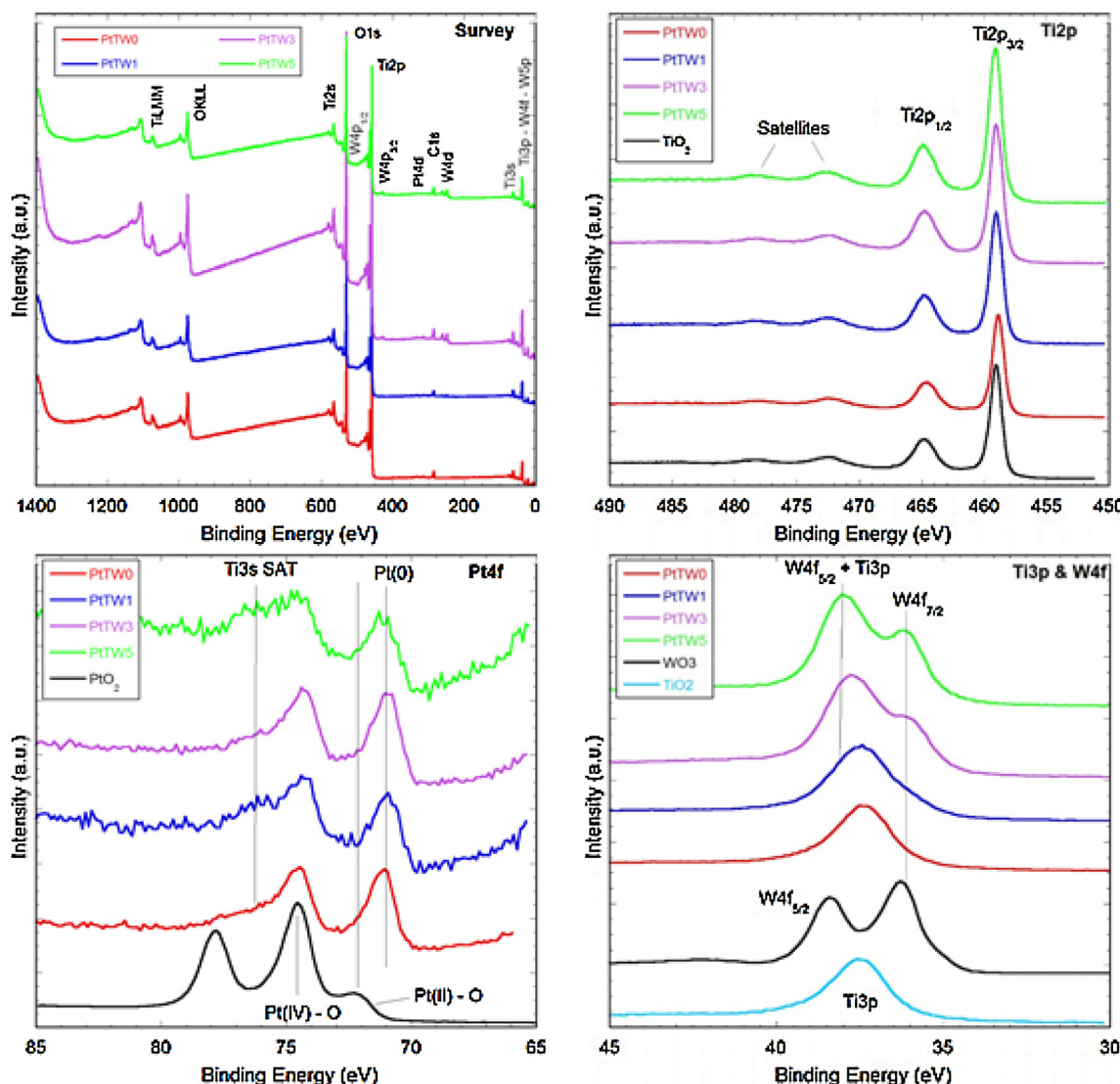


**Fig. 4.** XPS survey and high-resolution spectra of the investigated catalysts, in the Ti 2p, Pt 4f, Ti 3p and W 4f binding energy regions. X-ray Source: monochromatic Al K $\alpha$ .

**Table 3**

Results of 4-nitrostyrene (S) hydrogenation at 80% conversion in terms of selectivity to 4-aminostyrene (NH), formation rate of the latter ( $d[NH]/dt$ ) and 4-nitrostyrene conversion rate ( $-d[S]/dt$ ).<sup>a</sup>

Sample	Selectivity to NH	$d[NH]/dt$ (mmol g $^{-1}$ s $^{-1}$ )	$-d[S]/dt$ (mmol g $^{-1}$ s $^{-1}$ )
PtTW0	11%	0.0016	0.017
PtTW1	66%	0.057	0.078
PtTW3	53%	0.039	0.070
PtTW5	45%	0.027	0.050

<sup>a</sup> Reaction conditions: 80 °C, 10 bar of hydrogen, 0.67 mmol of 4-nitrostyrene in 20 g of toluene, with 50 mg of catalyst, in a 50 cm $^3$  autoclave.

content of tungsten is above 1%, the selectivity to 4-aminostyrene is slightly lower, i.e. 53 and 45% with PtTW3 and PtTW5, respectively, and the 4-nitrostyrene conversion rate is lower (see Table 3).

The higher selectivity to 4-aminostyrene with the tungsten-containing catalysts was consistent not only with an increased rate of 4-aminostyrene formation (see  $d[NH]/dt$  values in Table 3), but also with an increase in the overall rate of substrate conversion ( $-d[S]/dt$ ). A comparison of the results with PtTW0 and PtTW1 gave:

$$\Delta_{(d[NH]/dt)}(\text{PtTW1} - \text{PtTW0}) = 0.0554 \text{ mmol g}^{-1} \text{ s}^{-1}$$

$$\Delta_{(-d[S]/dt)}(\text{PtTW1} - \text{PtTW0}) = 0.0616 \text{ mmol g}^{-1} \text{ s}^{-1}$$

This indicates that the higher rate of 4-aminostyrene production ( $\Delta_{(d[NH]/dt)}$ ) is close to the higher overall rate of substrate conversion ( $\Delta_{(-d[S]/dt)}$ ). Thus, not only the selectivity in nitro group reduction is promoted by the presence of tungsten in the support, but also the observed increase in the conversion rate of the substrate ( $-d[S]/dt$ ) is mainly due to the higher rate of 4-aminostyrene production ( $d[NH]/dt$ ).

After longer reaction times (not shown) with the PtTWx oxides, 4-aminostyrene was fully converted into the completely hydrogenated 4-ethylaniline, with no phenyl-hydroxylamine derivatives present throughout the reaction.

### 3.3. Effects of the support oxide composition on the reaction rate and selectivity

With all tungsten-containing catalysts the formation of 4-ethylnitrobenzene, the main product obtained with PtTW0, took place at a much lower rate than with PtTW0, i.e. the selectivities to 4-aminostyrene and to 4-ethylnitrobenzene were reversed (Fig. 6b vs a).

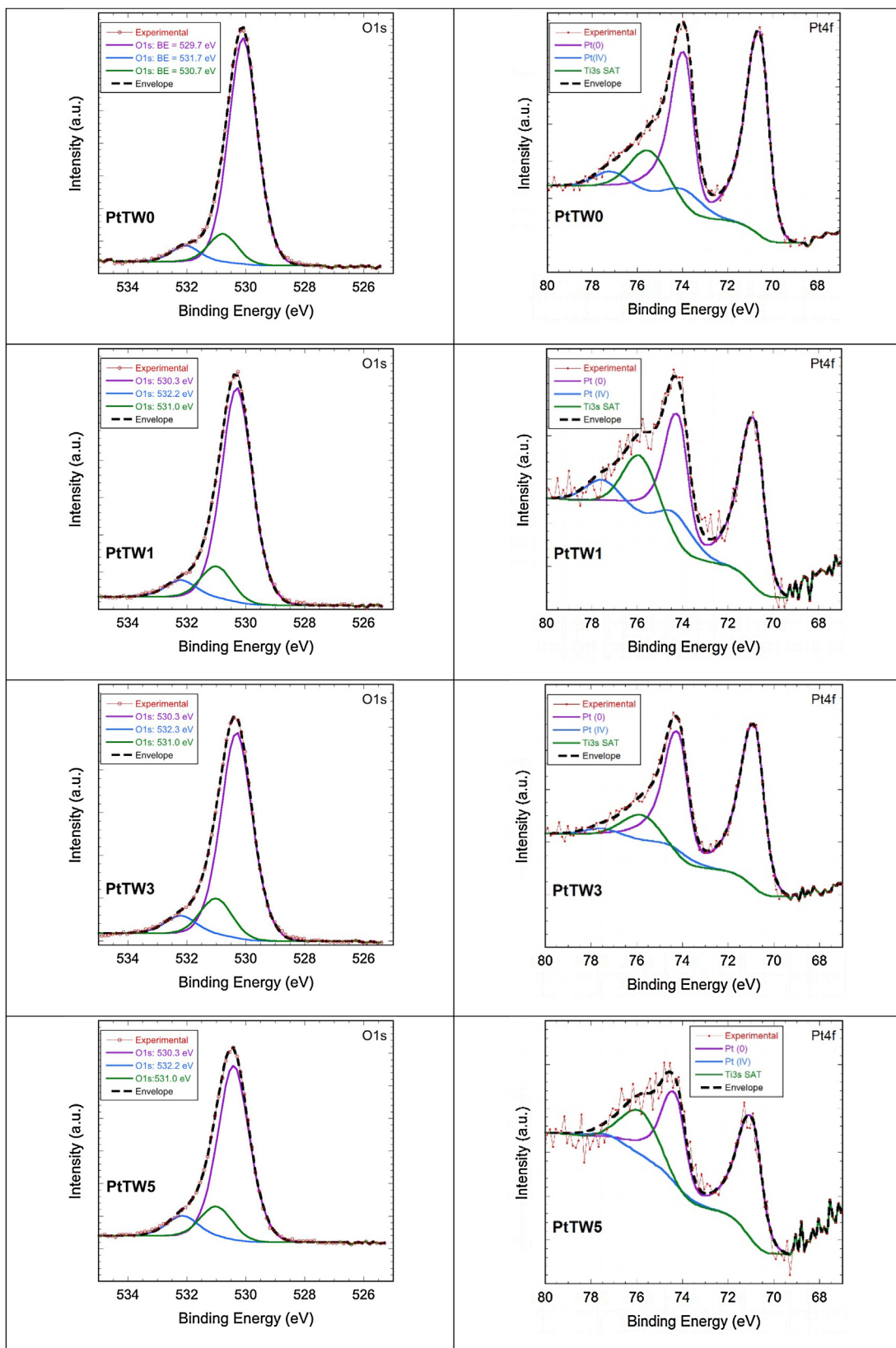
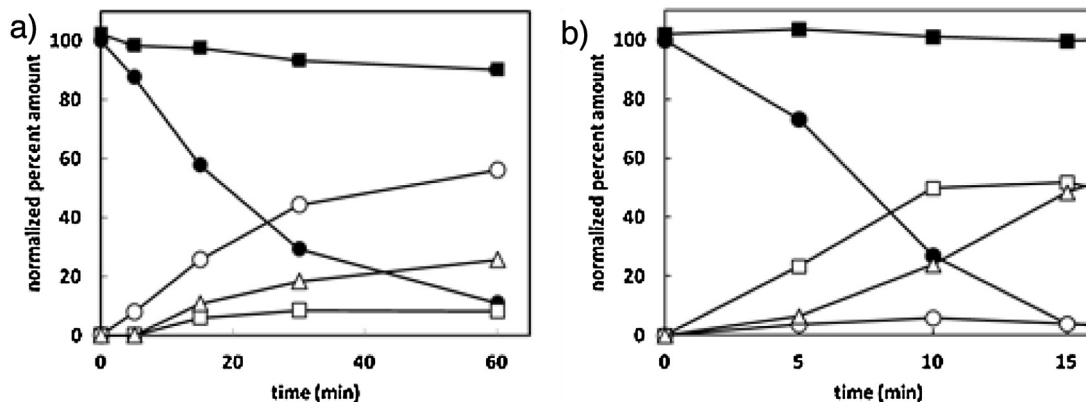


Fig. 5. O 1s and Pt 4f high-resolution X-ray photoelectron spectra.

Furthermore, with PtTW1 full conversion of the 4-nitrostyrene substrate was achieved within the first 15 min, i.e. in about a quarter of the time required when the reaction was carried out with PtTW0. Of particular importance is the linear decrease of 4-nitrostyrene

concentration with time (Fig. 6b), i.e. according to the zero order rate law, not with a positive order as with the tungsten-free catalyst (Fig. 6a). According to the Langmuir-Hinshelwood model, this



**Fig. 6.** Evolution of the 4-nitrostyrene substrate (●), of the intermediates and product, 4-ethynitrobenzene (○), 4-aminostyrene (□) and 4-ethylaniline (△), and carbon balance (■) in the liquid phase hydrogenation of 4-nitrostyrene on (a) PtTWO and (b) PtTW1. Reaction conditions: 80 °C, 10 bar of hydrogen. 0.67 mmol of 4-nitrostyrene in 20 g of toluene, with 50 mg of catalyst, in a 50 cm<sup>3</sup> autoclave.

implies that there is greater coverage of the substrate on the active sites of the catalyst in the tungsten-doped titania.

The higher activity of tungsten-containing catalysts originates, at least in part, from the greater specific surface area of the tungsten-containing materials. This effect is common to titania materials doped with different elements that stabilize the anatase phase [2]. The larger surface allows a greater dispersion of smaller platinum nanoparticles (Table 1). This is in line with the lower Pt/Ti ratios for the tungsten-containing catalysts determined by XPS analysis (Table S1) and is confirmed by the images shown in Figs. 1 and 2.

As demonstrated by Corma et al. [3] by carbon monoxide adsorption followed by IR spectroscopy, such smaller platinum nanoparticles have a smaller fraction of metal atoms in exposed faces with respect to atoms in the corner of crystallites. The same authors demonstrated that the rate of nitrobenzene hydrogenation on Pt/Al<sub>2</sub>O<sub>3</sub> is slightly affected by the amount (and consequently the size) of platinum particles on the alumina surface, while the rate of styrene hydrogenation increases with the amount of platinum on alumina, i.e. with increasing the fraction of facets on the platinum nanoparticles, where preferential adsorption through the aromatic and C=C moieties may occur. Thus in substituted nitroaromatics containing olefinic groups, such as 4-nitrostyrene, the chemoselectivity towards the reduction of the nitro group increases when the size of the platinum particles decreases. This contributes to the higher selectivity to 4-aminostyrene of the tungsten-containing catalysts, where smaller-sized platinum nanoparticles were photo-deposited.

Moreover, apart from size effects of platinum nanoparticles, the presence of tungsten in such catalysts also leads to a lower hydrophilicity of the oxide surfaces, as demonstrated by the disappearance of most of the OH surface groups, replaced by oxygen linked to tungsten (see Table 2). This indicates that in tungsten-containing oxides, tungsten not only substitutes titanium in the anatase lattice (Fig. 2), but is also present as WO<sub>x</sub> species on the mixed oxide surface, which possibly affect the size of the platinum particles photo-deposited on the mixed oxide support and the 4-nitrostyrene adsorption mode.

XPS analysis also indicate that Pt<sup>IV</sup> is stable in the metal nanoparticles when tungsten is present in the oxide support. In the XPS spectra measured after exposure to air, the signal of Pt<sup>IV</sup> shifts to positive binding energy (+0.4 eV) when tungsten is present in the support oxide (Table 2). Furthermore, whereas the BE of the W 4f signal appears to be unaffected by the smaller amounts of tungsten in the oxide support (Table 2), the O 1s signal, assigned to the hydroxyl groups bound to titania, shifts from 531.5 eV in

TWO to 530.7 eV (−0.8 eV) in the presence of platinum nanoparticles (PtTWO) and then further shifts back to 531.0 eV (+0.3 eV with respect to PtTWO) in tungsten-containing PtTW<sub>x</sub> ( $x > 0$ ) oxides. Thus, oxygen atoms appear to play a role in platinum-tungsten interactions, probably acting as W-O-Pt bridges between the two metals.

Reduction of Pt<sup>IV</sup> and W<sup>VI</sup> may occur under reaction conditions. It is worth underlining, however, that the best performing PtTW1 catalyst (Table 3) in terms of both 4-nitrostyrene conversion and selectivity to 4-aminostyrene exhibits the highest Pt<sup>IV</sup>/Pt<sup>0</sup> ratio.

A possible explanation of the maximum activity and selectivity attained with this catalyst is provided by the in-depth distribution analysis of platinum, which can be estimated non-destructively by XPS, by calculating the Pt 4f to Pt 4d area ratios, i.e. with an analysis based on two different core lines of the same element. The Pt 4d peaks are found at a kinetic energy of 1173.6 eV (BE 313 eV), the Pt 4f peaks at 1412.6 eV (BE 74 eV). Thus, the Pt 4f signals provide information to a greater depth than those of Pt 4d.

The area ratios of the two XPS signals were found to be 0.8 for sample PtTWO, in agreement with the theoretical value, 0.6 for sample PtTW1, 0.5 for PtTW3 and 0.4 for PtTW5. This finding seems to support the fact that the higher the tungsten content, the thicker the layer through which the Pt 4f photoelectrons travel until they leave the sample. These results lead to the conclusion that WO<sub>x</sub> is not only dispersed on the support, but it also covers the platinum nanoparticles. Assuming a core-shell model (about 2 nm Pt nanoparticles diameter), the thickness of the shell is estimated to range from 1.8 nm for PtTW1 to 3.0 nm for PtTW5. Thus the highest activity and selectivity obtained with the PtTW1 sample result from the preferential adsorption of 4-nitrostyrene through the nitro group on small platinum particles, which are only slightly covered by the WO<sub>x</sub> surface layer. With increasing the tungsten content of the catalysts, the WO<sub>x</sub> layer on platinum nanoparticles active sites would increase, and both activity and selectivity are expected to consequently decrease.

#### 4. Conclusions

Selective hydrogenation of 4-nitrostyrene to 4-aminostyrene is achieved by using platinum supported on tungsten oxide-doped titania. The presence of tungsten enhances the rate of reduction of the nitro group and suppresses that of the olefinic group, thereby changing the reaction from positive to zero order in 4-nitrostyrene. Tungsten stabilizes the smaller particle size of both titania and platinum, enhancing surface activity and the formation of Pt nanoparticles with a high number of metal sites in corners

and axes, on which 4-nitrobenzene preferentially adsorbs through the nitro group. The best performance, in both reaction rate and selectivity to 4-aminostyrene, of the PtTW1 mixed oxide support catalyst with a 1% W/Ti molar ratio results from an optimal combination of high surface area, small-sized platinum nanoparticles allowing the preferential adsorption of 4-nitrostyrene through the nitro group and low coverage of amorphous  $\text{WO}_x$  species on the platinum active sites.

## Acknowledgements

This work originates from the stage that MC made at the ICB of the ETH Zurich, as an Erasmus exchange Master student from the Department of Chemistry of the University of Milan. The authors are grateful to Prof. Nicholas Spencer (Laboratory for Surface Science and Technology, ETH Zurich) for access to the Surface Analytical Laboratory. Mr. Cossu carried out the technical maintenance of the spectrometers. Our thanks also go to the Electron Microscopy Centre, EMEZ, ETH Zurich, for the assistance in TEM measurements. The Sardinia Regional Government is gratefully acknowledged for financial support (P.O.R. Sardegna F.S.E. Operational Program of the Regione Autonoma della Sardegna, European Social Fund 2007–2013-Axis IV Human Resources, Objective 1.3, Line of Activity 1.3.1 “Avviso di chiamata per il finanziamento di Assegni di Ricerca”).

## Appendix A. Supplementary data

Supplementary data associated with this article can be found, in the online version, at <http://dx.doi.org/10.1016/j.apcata.2016.03.031>.

## References

- [1] H. Park, Y. Park, W. Kim, W. Choi, J. Photochem. Photobiol., C: Photochem. Rev. 15 (2013) 1–20.
- [2] M.V. Dozzi, E. Selli, J. Photochem. Photobiol., C: Photochem. Rev. 14 (2013) 13–28.
- [3] A. Corma, P. Serna, P. Concepción, J.J. Calvino, J. Am. Chem. Soc. 130 (2008) 8748–8753.
- [4] S.T. Marshall, M. O'Brien, B. Oetter, A. Corpuz, R.M. Richards, D.K. Schwartz, J.W. Medlin, Nat. Mater. 9 (2010) 853–858.
- [5] H.-U. Blaser, H. Steiner, M. Studer, ChemCatChem 1 (2009) 210–221.
- [6] J.A. Tafesh, J. Weiguny, Chem. Rev. 96 (1996) 2035–2052.
- [7] J.P. Adams, J. Chem. Soc., Perkin Trans. 1 (2002) 2586–2597.
- [8] R.S. Downing, P.J. Kunkeler, H. van Bekkum, Catal. Today 37 (1997) 121–136.
- [9] P. Lara, K. Philippot, Catal. Sci. Technol. 4 (2014) 2445–2465.
- [10] A. Corma, P. Serna, Science 313 (2006) 332–334.
- [11] M. Makosch, W.I. Lin, V. Bumbalek, J. Sa, J.W. Medlin, K. Hungerbuhler, J.A. van Bokhoven, ACS Catal. 2 (2012) 2079–2081.
- [12] J.D.M. Snelders, N. Yan, W. Gan, G. Laurenczy, P.J. Dyson, ACS Catal. 2 (2012) 201–207.
- [13] P. Serna, A. Corma, ACS Catal. 5 (2015) 7114–7121.
- [14] F. Riboni, L.G. Bettini, D.W. Bahnemann, E. Selli, Catal. Today 209 (2013) 28–34.
- [15] M.V. Dozzi, A. Saccomanni, M. Altomare, E. Selli, Photochem. Photobiol. Sci. 12 (2013) 595–601.
- [16] M.V. Dozzi, S. Livraghi, E. Giamello, E. Selli, Photochem. Photobiol. Sci. 10 (2011) 343–349.
- [17] M. Crobu, A. Rossi, F. Mangolini, N.D. Spencer, Anal. Bioanal. Chem. 403 (2012) 1415–1432.
- [18] R.D. Shannon, Acta Crystallogr. A 32 (1976) 751–767.
- [19] N.P. Huang, R. Michel, J. Voros, M. Textor, R. Hofer, A. Rossi, D.L. Elbert, J.A. Hubbell, N.D. Spencer, Langmuir 17 (2001) 489–498.
- [20] W. Hoffmann, T. Bormann, A. Rossi, B. Müller, R. Schumacher, I. Martin, M. de Wild, D. Wendt, J. Tissue Eng. 5 (2014) 1–14.
- [21] Q.N. Zhao, C.L. Li, X. He, X.J. Zhao, Key Eng. Mater. 29 (2013) 457–462.
- [22] A.M. Venezia, D. Duca, M.A. Floriano, G. Deganello, Surf. Interfaces Anal. 19 (1992) 543–547.
- [23] A. Lewera, L. Timperman, A. Roguska, N. Alonso-Vante, J. Phys. Chem. C 115 (2011) 20153–20159.
- [24] K.P. Pernstich, M. Schenker, F. Weibel, A. Rossi, W.R. Caseri, ACS Appl. Mater. Interfaces 2 (2010) 639–643.
- [25] D. Atzei, A. De Filippo, R. Rossi, C. Sadun, Inorg. Chim. Acta 248 (1996) 203–208.
- [26] D. Atzei, D. De Filippo, A. Rossi, M. Porcelli, Spectr. Acta A 57 (2001) 1073–1083.
- [27] F.B. Li, X.Z. Li, Chemosphere 18 (2002) 1103–1111.
- [28] K.S. Kim, N. Winograd, Chem. Phys. Lett. 31 (1975) 312–317.
- [29] G. Orsini, V. Tricoli, J. Mater. Chem. 21 (2011) 14530–14542.